3D tensegrity braces with superelastic response for seismic control

Filipe Santos, Catarina Caroço, Ada Amendola, M. Miniaci, Fernando Fraternali

3D tensegrity braces with superelastic response for seismic control

Filipe Santos[1], Catarina Caroço[1], Ada Amendola[2], Marco Miniaci[4], and Fernando Fraternali[2]

[1] CERIS, Department of Civil Engineering, Universidade NOVA de Lisboa, Quinta da Torre, 2829-516 Caparica, Portugal

[2] Department of Civil Engineering, University of Salerno, Via Giovanni Paolo II, 132, Fisciano (SA), 84084, Italy

[3]CNRS, Univ. Lille, Centrale Lille, Univ. Polytechnique Hauts-de-France, Junia, UMR 8520 -IEMN, F-59000 Lille, France

November 20, 2021

Abstract

Tensegrity structures have recently shown great potential as bracing devices for seismic control due to their unique ability to passively dissipate energy in structures subjected to severe deformations. Indeed, behaving as nonlinear springs, they are able to dissipate a great amount of energy energy during mechanical loading-unloading cycles. Planar tensegrity D-bar systems composed of four bars forming a rhombus, internally stabilized through a set of two perpendicular Shape Memory Alloy (SMA) cables, represent excellent candidates to act as braces for seismically resistant structures. However, although their tapered configuration maximizes in-plane buckling resistance with minimal mass, the out-of-plane buckling of such systems can compromise their overall structural efficiency, potentially engendering damage into adjacent non-structural elements. In this paper, the efficiency of three-dimensional D-bar tensegrity structures under compressive loads is examined with the aim of proposing an advantageous design of D-bar-based bracing systems with optimized masses. We show that, by introducing a pre-strain in the superelastic cables, it is possible to achieve a wide shaped hysteresis, which yields to a significant amount of equivalent viscous damping (up to 30%). The presented numerical results on the energy dissipation properties of the examined structures, corroborated by experimental measurements of the buckling response, shed light on the research field of three-dimensional tensegrity structures, as efficient and lightweight bracing devices for seismic control.

Keywords: Bracing systems, Tensegrity structures, Seismic Control, Buckling Response, Energy Dissipation, Shape Memory Alloy, 3D printing, Eco-friendly materials.

Introduction

Recent studies have highlighted the great potential of tensegrity units when acting as bracing devices for seismic control [1, 2]. It is well known that dissipative bracing systems provide efficient tools to passively dissipate energy in structures that are subject to severe earthquakes [3]-[12]. Indeed, such systems interacts with the structure behaving as nonlinear springs, and are able to dissipate energy during mechanical loading-unloading cycles.

In this context, it has been shown that D-bar tensegrity systems (TSs) can achieve large buckling load to mass ratios along with a very high energy storage capacity with minimal mass [13, 14, 15]. By equipping the D-bar bracing systems with shape-memory alloy (SMA) cables [1, 2], it is possible to dissipate a large amount of energy based on the superelastic effect [16, 17, 18], which results into a reversible strain during cyclic loading–unloading, associated with a wide stress hysteresis.

Due to its geometric nonlinearities, the D-bar brace is able to strongly amplify the applied longitudinal displacement in the transverse direction, allowing the transverse SMA cables to experience marked axial

strain, fostering high martensitic transformation ratios and high dissipation features. In what follows, let 'CxTy' denote a TS composed of x compressed members (C) and y tensile members (T).
In literature [15] it has been shown that planar tensegrity D-bar systems composed of four bars forming a rhombus, internally stabilized through a set of two perpendicular SMA cables (C4T2) can perform very well as braces for seismically resistant structures, aimed to prevent or minimize structural damage during earthquakes.
However, although their tapered configuration maximizes in-plane buckling resistance with minimal mass, the out-of-plane buckling of the C4T2 D-bar brace can compromise its overall structural efficiency and may also cause damage to adjacent non-structural elements. A possibility to mitigate this problem is to design the cross-section of the struts in such a way that their out-of-plane slenderness is lower than the in-plane one. Another alternative to improve the performance of the planar device, is to consider a three-dimensional version of the D-bar brace, made of six bars, one longitudinal SMA cable and a set of three transverse SMA cables, forming a triangular bipyramid (C6T4). The geometry of the systems illustrated above and that will be explored in this paper is shown in Figure 1, where a straight column (a), the planar C4T2 (b) and a three-dimensional (C6T4) tensegrity D-bar systems are reported, respectively.

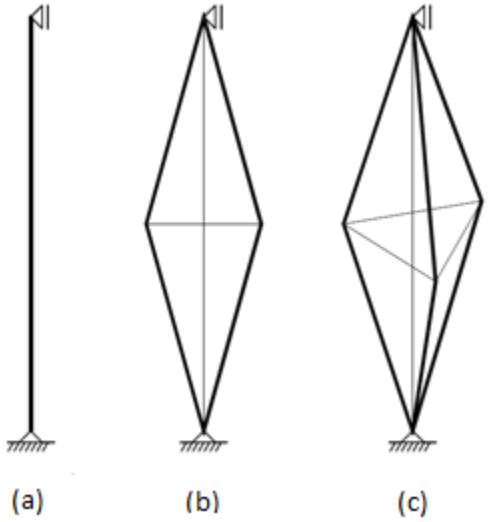

Figure 1: Tensegrity inspired D-bar bracing systems of different complexities: (a) Straight column, (b) C4T2, and (c) C6T4.

1 Mechanical modeling of D-bars

In this section we evaluate the efficiency of D-bar tensegrity structures under compressive loads in order to design bracing systems with optimized masses. We start by defining the Euler buckling conditions for a single straight bar (Figure 1, a) and then we replace the single bar by C4T2 (Figure 1, b) and C6T4 (Figure 1, c) systems.
We assume that the bars of the D-braces behave as rigid bodies during any arbitrary transformation of the structure in the pure stretching regime that precedes the occurrence of buckling events. This assumption is commonly accepted when dealing with tensegrity structures, in which the axial stiffness of the bars is markedly greater than the one of the strings (see, e.g. [13]).
At first, we compare the buckling response of a planar C4T2 brace with that of a straight column with equal length ℓ_0, which is made out of the same material of the bars forming the TS. For the sake of simplicity, we assume that both the straight column and the struts of the C4T2 brace have circular cross-sections. The Eulerian buckling load of the straight beam is easily computed as:

$$P_{cr} = \pi^2 E r_0^4/(4\ell_0^2) \tag{1}$$

where E denotes the Young's modulus characterizing the elastic response of the material in the post-buckling regime, and r_0 the radius of the beam.
One can solve Eqn. (1) for r_0, obtaining the mass m_0 of the beam as:

$$m_0 \;=\; \varrho\,\pi\,r_0^2\,\ell_0 \;=\; 2\,\varrho\,\ell_0^2\,\sqrt{P_{cr}/(\pi E)} \tag{2}$$

ϱ denoting the density of the material.
We now want to design the mass of the bars forming the C4T2 brace, shown in Figure 2 so that such a structure exhibits the same buckling load of the straight column under examination. We assume that the strings forming the brace go slack when loaded in compression. The bar mass of D-braces is usually nearly coincident with the overall mass of the structure, due to the lightweight nature of the cables.

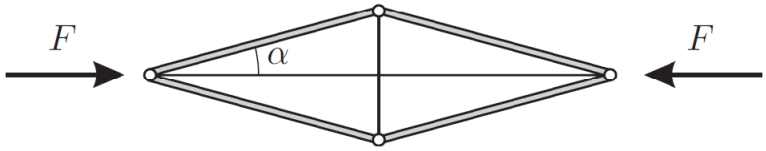

Figure 2: C4T2 D-bar system.

The Eulerian buckling load of each bar forming the C4T2 brace is computed as:

$$N_{cr} \;=\; \pi^2 E r_1^4/(4k^2\ell_1^2) \tag{3}$$

where r_1 and ℓ_1 are the radius and the length of the struts, respectively and k is a factor that translates the buckling length of the strut. Setting $N_{cr} = P_{cr}/(2\sin\alpha)$, and solving Eqn. (3) for r_1, it is possible to show that:

$$m_1 \;=\; 4\;k\times 2\varrho\;\ell_1^2\;\sqrt{N_{cr}/(\pi E)} \;=\; k\;m_0\;(2\sin^5\alpha)^{-\frac{1}{2}} \tag{4}$$

One therefore gets:

$$\mu_1 = m_1/m_0 \;=\; k\;(2\sin^5\alpha)^{-\frac{1}{2}}, \tag{5}$$

in the infinitesimal displacement regime, with m_0 representing the mass of the original straight column and m_1 the mass of the C4T2. Equation (5) yields to a m_1/m_0 ratio smaller than one when $\alpha < 29.5$ degrees, if $k = 1$, i.e., if we consider in-plane buckling of the C4T2 brace. This is quite a remarkable result, that shows that a C4T2 brace with tapered profile ($\alpha \ll 29.5$ degrees) exhibits a significantly greater buckling load, as compared to a straight column of equal mass. However, if we consider the possibility of out-of-plane buckling (with $k = 2$), this geometric advantage disappears. Here lies one of the motivations of this work, which is to explore the enhanced buckling resistance provided by the three-dimensional arrangement obtained with the C6T4 D-brace. It can be shown that the generalization of Eqn. (5), for the C6T4 case results in:

$$\mu_2 = m_2/m_0 \;=\; (\frac{4}{3}\sin^5\alpha)^{-\frac{1}{2}}, \tag{6}$$

with m_2 representing the mass of the C6T4 bracing. Equation (6) yields to a m_2/m_0 ratio smaller than one when $\alpha < 19.3$ degrees. In Figure 3 the mass reduction curves obtained for the considered D-bar braces are shown as a function of α.

One can confirm that it becomes impossible to optimize the mass of a C4T2 bracing susceptible to out-of-plane buckling and that, for $\alpha < 19.3$ degrees, the C6T4 serves as a good alternative to tackle this problem.

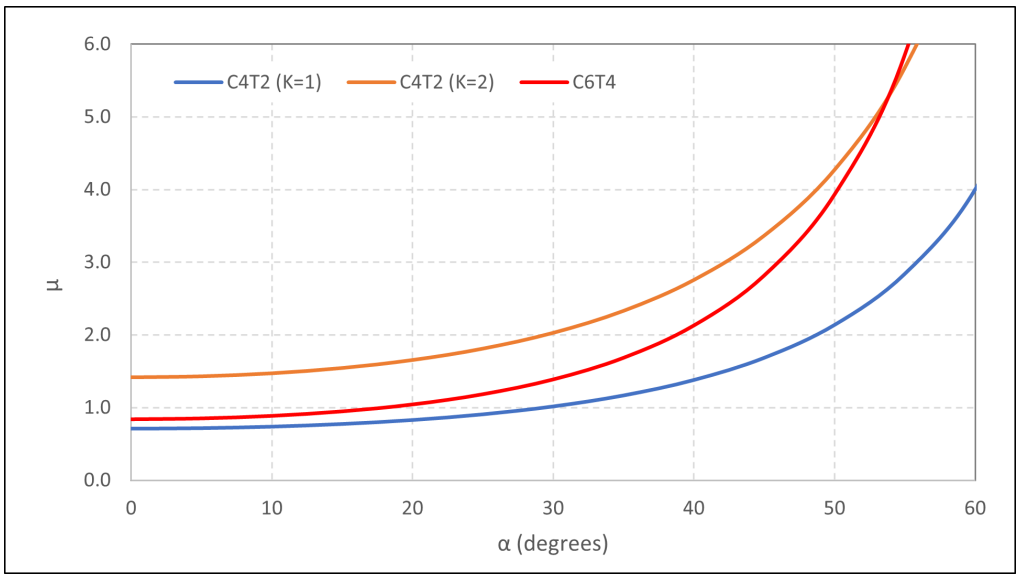

Figure 3: Mass reduction curves for the D-bar bracing systems.

2 Experimental study of the buckling behavior

In this section, a series of experimental tests are performed to characterize the buckling behavior of 2D and 3D D-Bar braces, using the straight column case as a benchmark.

2.1 Geometries

The length of the benchmark straight column was defined according to the dimension of the diagonal of the print table of a standard 3D printer, yielding a total of 270 mm between the support points. The design slenderness of the column was set to $\lambda = 90$, and a diameter of 12 mm was obtained. The buckling load of the benchmark column was then calculated and three different D-bar braces were designed in order to present the same buckling resistance. The design criteria for the D-bar braces was defined as follows: a light C4T2 D-bar system, designed for $k = 1$, not taking into consideration the out-of-plane buckling problem (see Figure 4(a)); a heavy C4T2 D-bar system, designed for $k = 2$; (see Figure 4(b)) and a C6T4 D-bar system. The geometric parameters and masses of the considered bracing systems are listed in Table 1, for an angle α of 15 degrees. The theoretical buckling resistance of all the systems is the same, amounting to 375 N.

Table 1: **Bracing systems parameters.**

Bracing system	strut length mm	diameter mm	mass g
Straight column	270	12.00	374
C4T2 (light)	140	7.32	289
C4T2 (heavy)	140	10.36	577
C6T4	140	6.62	354

2.2 Materials and methods

All the bracings analyzed in this work were manufactured by processing spools of commercial, eco-sustainable PLA filaments distributed by Fillamentum® (https://fillamentum.com) with 1.75 mm diameter, using a Prusa i3 MK2 3D printer by Prusa Research (https://www.prusa3d.com/) with a

0.4 mm diameter nozzle. The printing parameters used to fabricate the 3D-printed specimens are listed in Table 2.

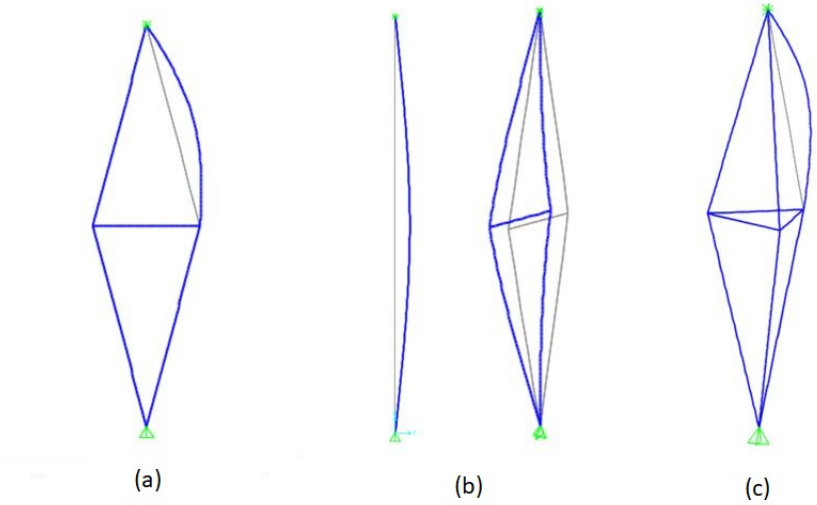

Figure 4: Buckling modes for the C4T2 and C6T4 braces: (a) C4T2, in-plane; (b) C4T2, out-of-plane; (c) C6T4.

Figure 5: 3D printed braces: (a) Straight column; (b) light 2D D-bar; (c) heavy 2D D-bar; (d) 3D D-bar.

In order to obtain optimized bracings in terms of mass, an infill percentage of 50% was used to print the specimens, with 2 solid outer shells. In the connection zones, the infill percentage was 100%. The specimens were than weighted, presenting the following masses: m(straight column) = 0.220 kg; m(C4T2 (light))= 0.210 kg; m(C4T2 (heavy)) = 0.380 kg and m(C6T4) = 280 kg. The 3D printed bracing systems are presented in Figure 5. Special design restraining pieces were introduced in the D-bars in order to obtain the buckling loads for the desired modes. A Zwick-Roell Z50 universal

Table 2: **3D printing parameters.**

Nozzle extrusion temperature	210 °
Heated bed temperature	60 ° C
Layer height	0.2 mm
Printing speed	30 mm/s
Number of outer shells	2

testing machine was used to perform the uniaxial compression tests on the 3D printed specimens. The extremities of the bracings were tightly secured into the testing grips with specially designed pieces, and the bracings were then compressed with a loading rate of 0.1 mm/s. One can see the layout of the uniaxial compression tests for all the specimens in Figure 6.

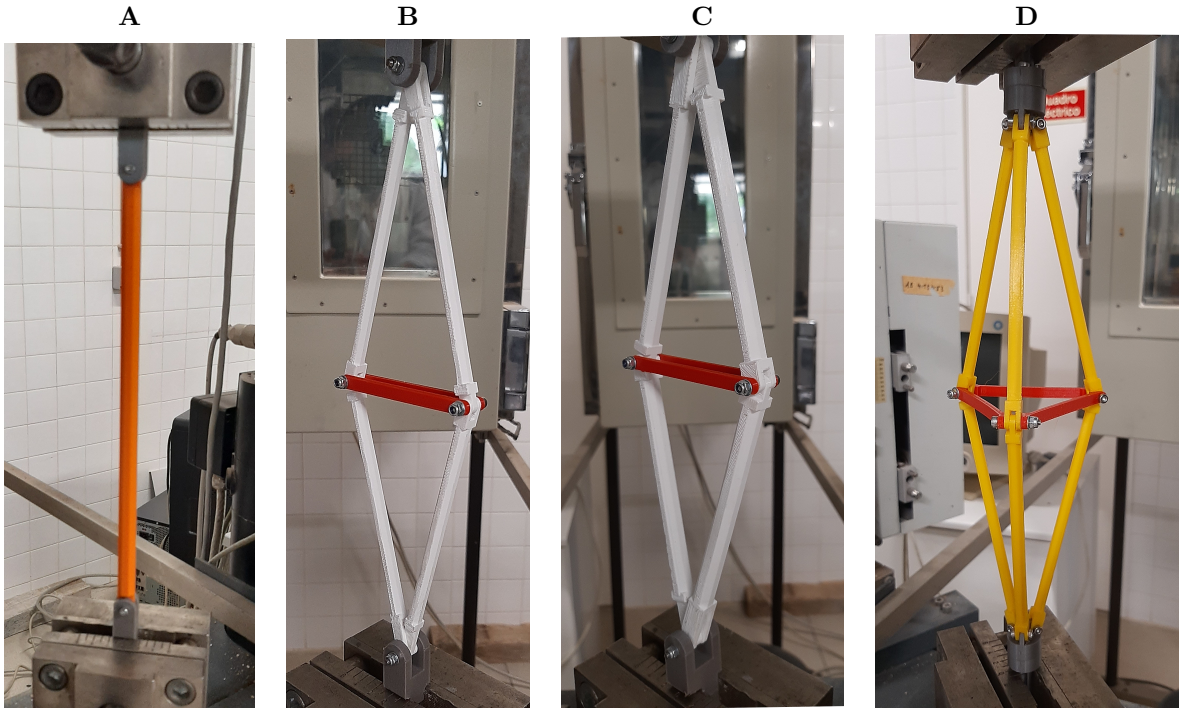

Figure 6: Uniaxial compression tests setup. (**A**) Straight column. (**B**) Light 2D D-bar. (**C**) Heavy 2D D-bar. (**D**) 3D D-bar.

2.3 Results

The post-buckling configurations for the 3D printed specimens are depicted in Figure 7. The force-displacement curves obtained during the uniaxial compression tests are plotted in Figure 8, for all the tested specimens. We can see from the results in Figures 7-8 that the buckling resistances are lower than the calculated theoretical results, especially in the case of the benchmark straight-column and the light C4T2 system. The fact that a 50% infill was implemented naturally contributed to the decreased buckling resistance of the specimens. In the case of the light C4T2 system, the theoretical out-of-plane buckling load amounted to 90 kN. One of the main problems observed in these planar systems relates with the low transversal stiffness of the nodes, which are materialized by thin plates that bend easily.

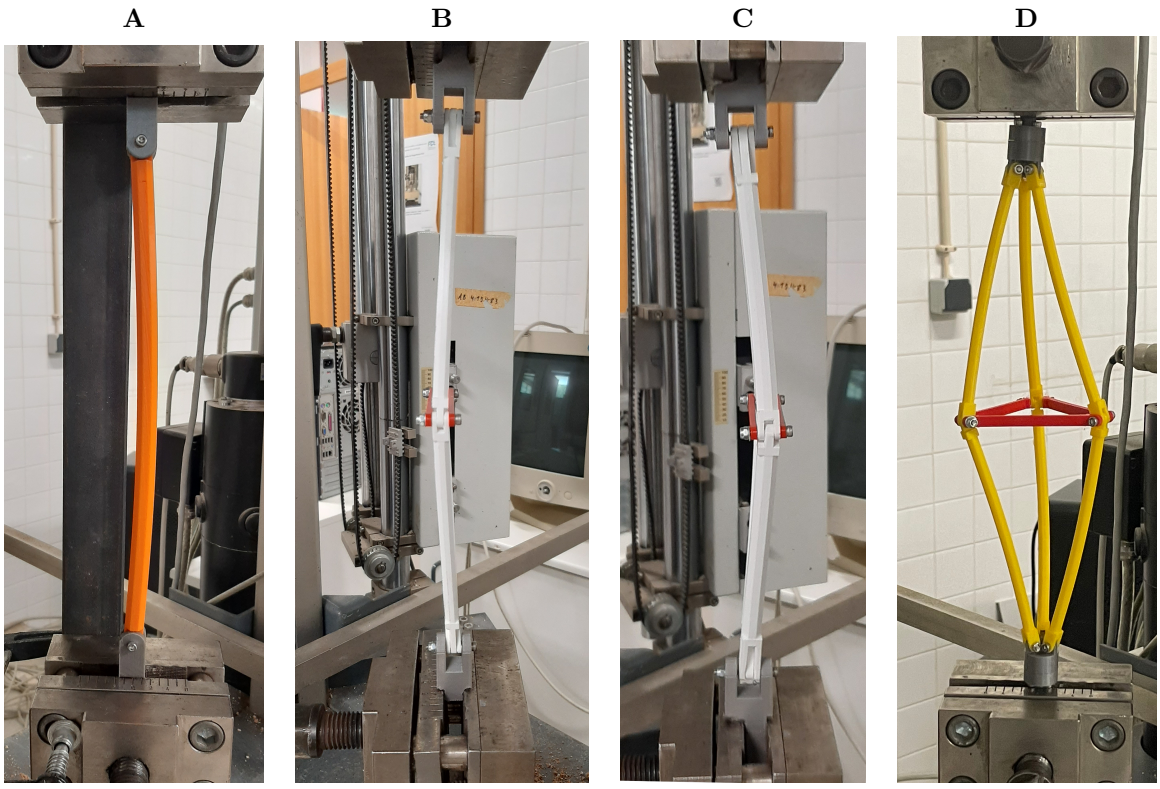

Figure 7: Post-buckling configurations. (**A**) Straight column. (**B**) Light 2D D-bar. (**C**) Heavy 2D D-bar. (**D**) 3D D-bar.

In general, the results are consisted with the predicted trends, with the heavy C4T2 system showing a higher buckling resistance than the benchmark straight-column, but at the cost of an extremely high mass. As expected, the C6T4 brace is the one showing higher buckling resistance. In order to make the comparison between the printed specimens more fair, we divided the obtained force-displacement diagrams by the mass of each bracing system and plotted the results in Figure 9. We can see that the better performance of the C6T4 bracing holds, and that the heavy C4T2 system is penalized by its high mass. We have shown the advantages of the C6T4 regarding its minimal mass features during compression. Now, we will focus on the great geometric advantage of the C6T4 system which is the possibility to easily introduce additional damping in the system by providing it with SMA tendons.

3 Numerical simulation of the energy dissipation capacity

The experimental results presented in the previous section have highlighted the enhanced buckling response of the three-dimensional C6T4 brace. We deal in the present section a numerical investigation on the energy dissipation properties of such a bracing system, using an ad hoc developed computational code that handles tensegrity systems equipped with SMA tendons (Figure 3). Taking advantage of the displacement amplification features shown by the C6T4 bracing it is possible to tailor its configuration in order to explore the full length of the martensitic transformation in its SMA superelastic tendons. A 4.0 m wide by 3.0 m tall structural frame is used to perform numerical tests on the C6T4 D-bar, yielding a bracing with a total length of 5000 mm.

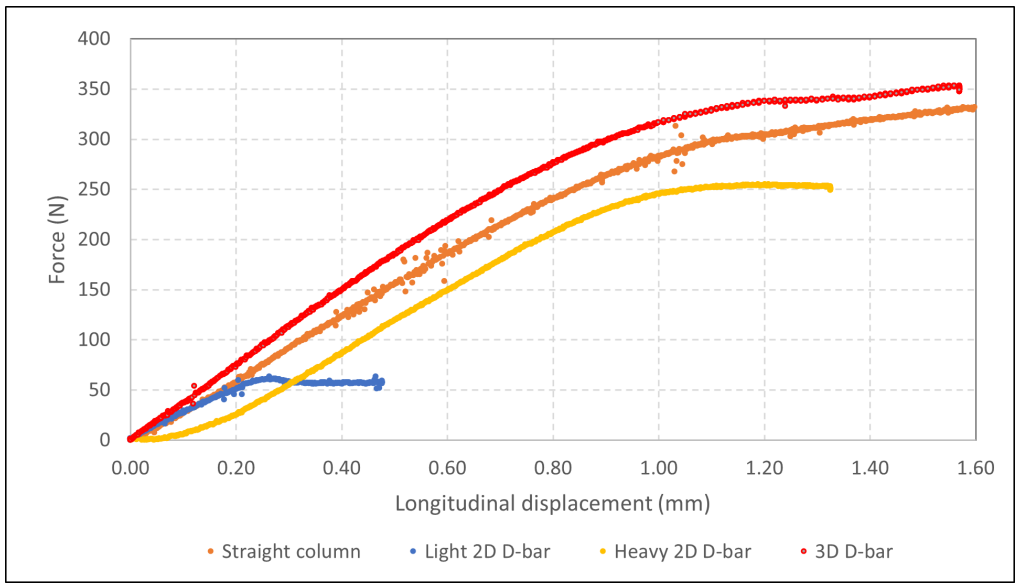

Figure 8: Force-displacement curves during uniaxial compression tests.

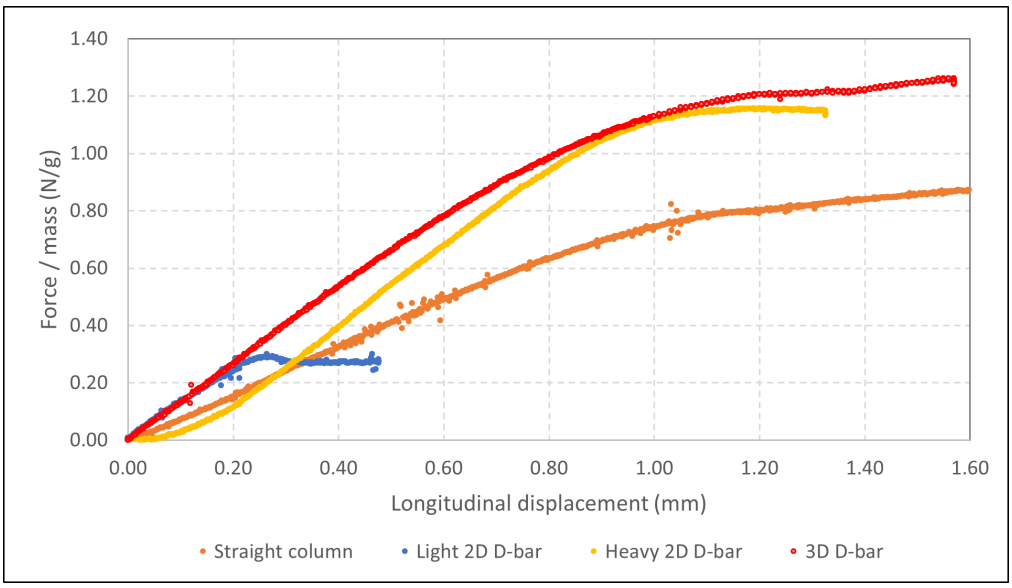

Figure 9: Normalized force-displacement curves recorded during uniaxial compression tests.

By basic trigonometric and arithmetic operations, it can be shown that it is possible to define the length of the transversal tendons (L_{SMA}), as a function of the total length of the bracing ($L_{bracing}$), the imposed longitudinal displacement (ΔL) and the desired objective design strain. (L_{SMA}) can be hence computed according to $L_{SMA} = (\Delta L.L_{bracing}/\varepsilon_{obj})^{1/2}$. By using the HAZUS definition of average inter-story drift (ISD) ratio of structural damage states we can set a maximum threshold for ΔL so as to obtain a slight damage state (0.6%) for a structure associated with low-rise buildings and a Moderate-Code design level. For an ISD of 0.6%, ΔL yields 14.4 mm. In order to prevent slackening of the superelastic cables during mechanical cycling and foster the full development of the martensitic transformation, we introduce an initial pre-strain in the cables of 3.2%. This means that we have an additional 3% strain up to the full completeness of the martensitic transformation in the cables, which amounts to about 6%. From then on, we will be elastically loading detwinned martensite. With these input parameters, we obtain $L_{SMA} = 1300$ mm. The superelastic restraining elements were assumed to be built up of 10 small cables of 1 mm diameter each. The remaining variables that allow for the full material characterization of the superelastic elements, which were used during the numeric

simulations, are listed in Table 3. Another feature of the model is that we have computed the lengths and the cross-section of the longitudinal SMA tendons in order to yield the same strains and stresses then the transverse ones, as shown in Figure 3(**B**). This leads to a much more effective bracing, with symmetric behavior during a mechanical cycle of tension and compression. After the introduction of the initial pre-strain, as shown in Figure 3(**A**), the C6T4 brace was subjected to a mechanical cycle up to a 6.3% strain. The force-displacement of the system subjected to the prescribed cyclic loading is shown in Figure 12.

Table 3: **Superelastic parameters**

M_f	- 45 º C	(martensite finishing temperature at zero stress)
M_s	- 35 º C	(martensite starting temperature at zero stress)
A_s	- 15 º C	(austenite starting temperature at zero stress)
A_f	- 5 º C	(austenite finishing temperature at zero stress)
E_M	20000 MPa	(martensite Young's modulus)
E_A	35000 MPa	(austenite Young's modulus)
$C_M = C_A$	6.5 MPa º C $^{-1}$	(Clausius-Clapeyron coefficients)
Θ	0 MPa º C C^{-1}	(thermoplastic coefficient)
ε_L	0.04	(recoverable strain)

During the numerical testing of the C6T4 bracing unit, with superelastic cables working in phase opposition, we show that, even for the small ISD introduced in the structure (0.6%), the cables are able to develop the characteristic flag shaped stress-strain diagrams associated with the superelastic behaviour. By introducing a pre-strain in the superelastic cables it is possible to obtain a wide shaped hysteresis, like the one shown in Figure 12, which yields a significant amount of energy dissipation capacity measured as equivalent viscous damping (30%). This damping is evaluated by the ratio of the dissipated energy during a mechanical cycle, which corresponds the area enclosed by the hysteresis, and the maximum strain energy multiplied by 4π. A high dissipation capacity of the brace permits to control the seismic response of the served structure, being particularly useful to mitigate the relative displacements between the structure and the ground on occasion of earthquakes [19].

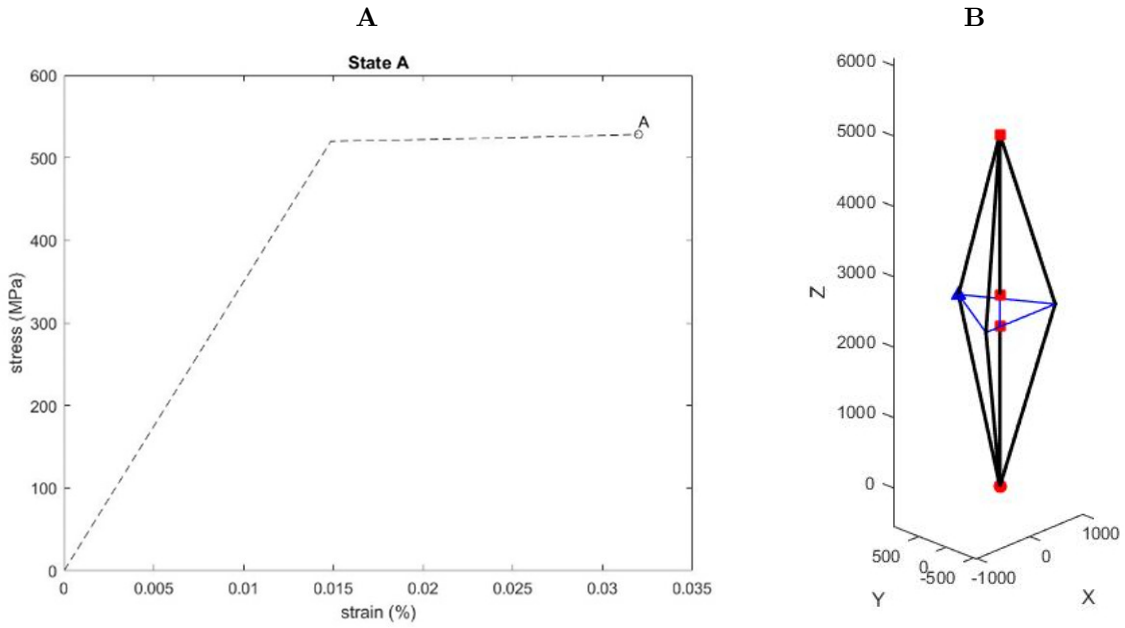

Figure 10: (**A**) Initial pre-strain state. (**B**) Computational model of the C6T4 brace.

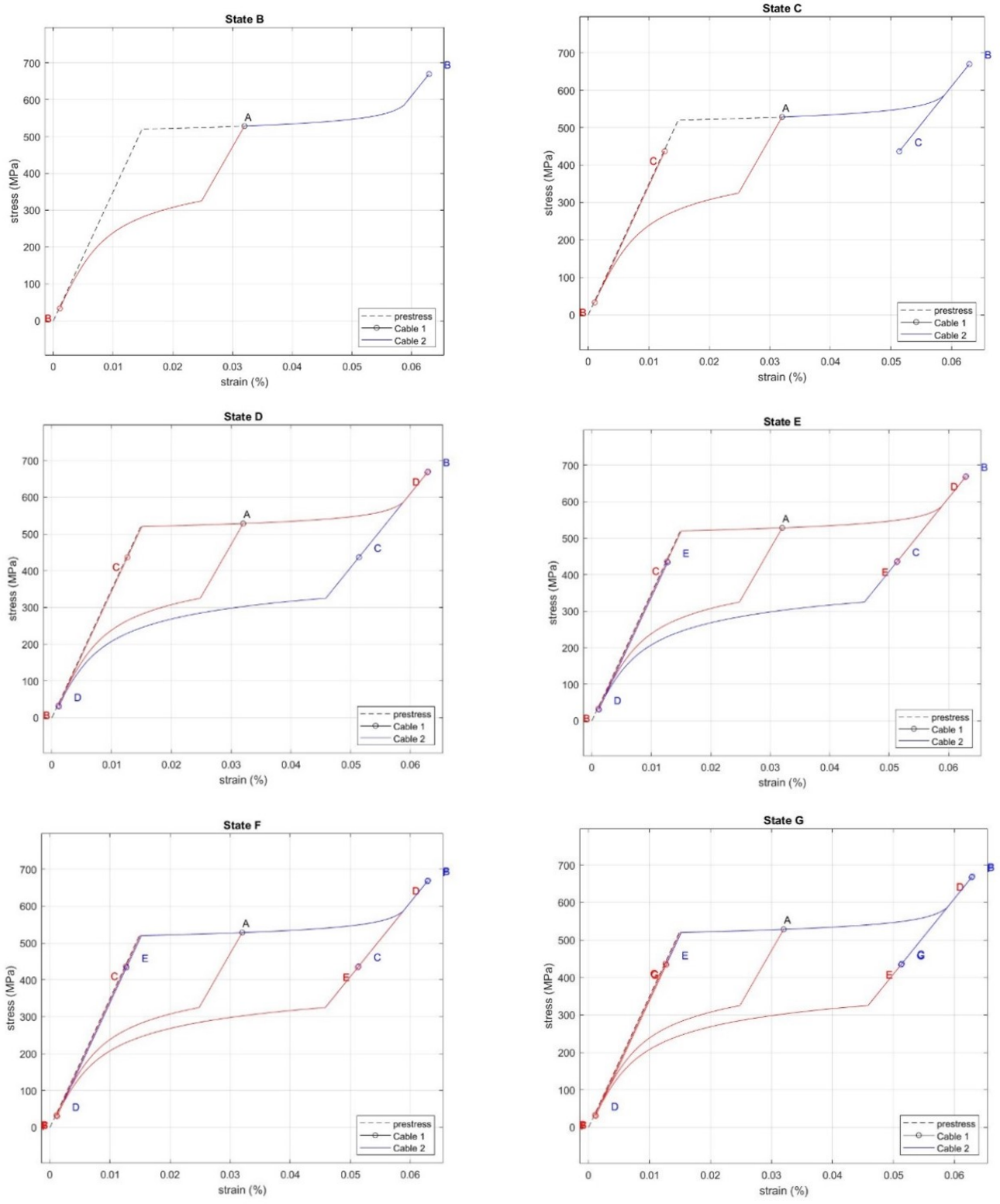

Figure 11: Numerical stress-strain curves of the SMA cables.

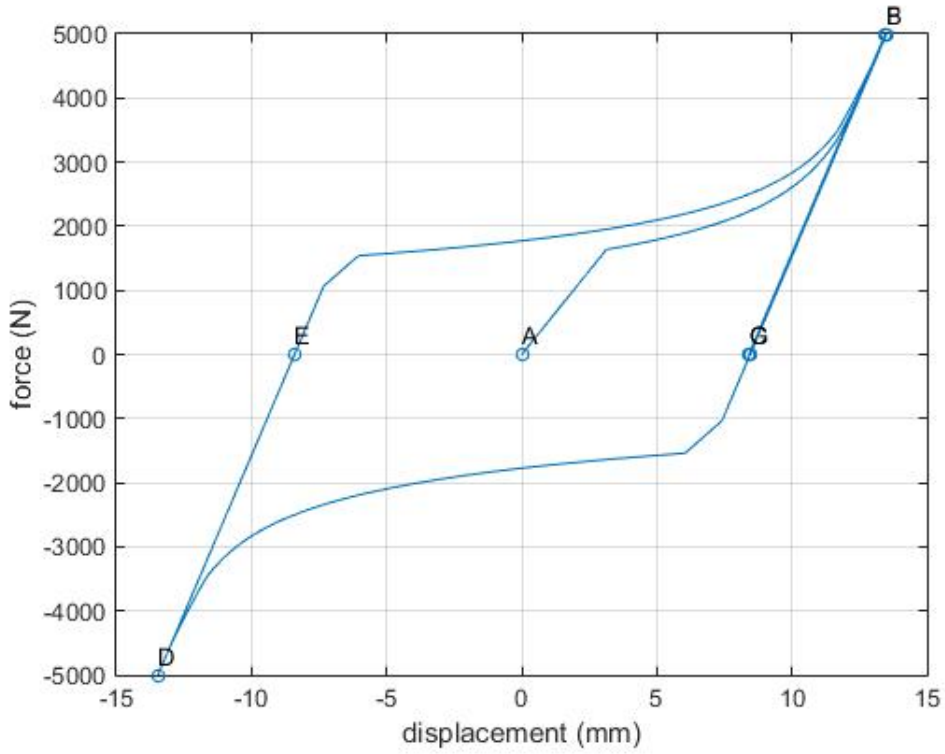

Figure 12: Numerical force-displacement curve for the C6T4 brace.

4 Concluding remarks

In this paper, we have numerically and experimentally investigated the efficiency of D-bar tensegrity structures under compressive loads with the aim of proposing an advantageous design of D-bar-based bracing systems with optimized masses. In particular, we have shown that a planar C4T2 brace with tapered profile ($\alpha \ll 29.5$ degrees) exhibits a significantly greater buckling load, as compared to a straight column of equal mass. However, if the possibility of out-of-plane buckling is considered, this geometric advantage disappears. To limit this problem, we have explored and proposed an enhanced buckling resistance mechanism provided by a three-dimensional arrangement obtained via a C6T4 D-brace.

We have showed that it is possible to achieve important values of energy dissipation capacity, measured through equivalent viscous damping, by introducing a suitable pre-strain in the superelastic cables, responsible for wide shaped hysteresis cycles. Experimental measurements, performed on additive manufactured samples, confirmed the numerical calculations, and unequivocally prove the superior properties of the proposed C6T4 D-brace system. The examined braces can be easily manufactured in a fabrication lab on employing SMA cables and parts 3D printed in eco-friendly materials [20]. Future directions of the present research will include an experimental validation of the energy dissipation properties of 3D tensegrity braces, as well as the design, mechanical modeling and testing of mechanical metamaterials obtained by tessellating such systems in three dimensions.

Funding

FF greatly acknowledges financial support through the Italian Ministry of University and Research PRIN 2017 grant 2017J4EAYB.

Competing interests

The authors declare that they have no conflict of interest.

Data availability

The stereolithography (STL) files of all the 3D printable parts of the analyzed braces can be provided by the corresponding author upon request.

References

[1] Santos, F., Benzoni, G., Fraternali, F., Seismic performance of superelastic tensegrity braces. *Ingegneria sismica/international journal of earthquake engineering*, vol. **36**, no. 3, pp. 20-37, 2019.

[2] Fraternali, F., Santos, F., Mechanical modeling of superelastic tensegrity braces for earthquake-proof structures. *Extreme Mech. Lett.*, vol. **33**, 100578, 2019.

[3] Mazzolani, F.M., Della Corte, G., D'Aniello, M., Experimental analysis of steel dissipative bracing systems for seismic upgrading. J. Civ. Eng. Manag., vol. **15**, 2009.

[4] Menna, C., Auricchio, F., Asprone, D., Applications of shape memory alloys in structural engineering. In: Concilio L, Lecce A, editors. Shape memory alloy engineering. Boston: Butterworth-Heinemann, vol. **13**, pp. 369–403, 2015.

[5] Chang, W., Araki, Y., Use of shape-memory alloys in construction: A critical review. *P I Civil Eng: Civil Engineering*, vol. **169**, no. 2, pp. 87-95, 2016.

[6] Walter Yang, C., DesRoches, R., Leon, R. T., Design and analysis of braced frames with shape memory alloy and energy-absorbing hybrid devices. *Eng. Struct.*, vol. **32**, no. 2, pp. 498-507, 2010.

[7] Miller, D.J., Fahnestock, L.A., Eatherton, M. R., Development and experimental validation of a nickel-titanium shape memory alloy self-centering buckling-restrained brace. *Eng. Struct.*, vol. **40**, pp. 288-298, 2012.

[8] Asgarian, B., Salari, N., Saadati, B., Application of intelligent passive devices based on shape memory alloys in seismic control of structures. *Structures*, vol. **5**, pp. 161-169, 2016.

[9] Bosco, M., Marino, E.M., Rossi, P.P., A design procedure for pin-supported rocking buckling-restrained braced frames. *Earthq. Eng. Struct. D*, vol. **47**, no. 14, pp. 2840-2863, 2018.

[10] Liu, M., Zhou, P., Li, H., Novel self-centering negative stiffness damper based on combination of shape memory alloy and prepressed springs. *J. Aerospace Eng.*, vol. **31**, no. 6, 2018.

[11] Dolce, M., Cardone, D., Marnetto, R., Implementation and testing of passive control devices based on shape memory alloys. *Earthq. Eng. Struct. D*, vol. **29**, no. 7, pp. 945-68, 2000.

[12] Das, S., Mishra, S.K., Optimal performance of buildings isolated by shape-memory-alloy-rubber-bearing under random earthquakes, *Int. J. Comput. Meth. Eng. Sci. Mech.*, vol. **15**, no. 3, pp. 265-276, 2014.

[13] Skelton, R.E., de Oliveira, M.C., Tensegrity Systems, *Springer*, 2010.

[14] Montuori, R., Skelton, R.E., Globally stable tensegrity compressive structures for arbitrary complexity, *Compos. Struct.*, vol. **179**, pp. 682–694, 2017.

[15] Goyal, R., Perrera Hernandez, E.A., Skelton, R.E., Analytical study of tensegrity lattices for massefficient mechanical energy absorption, *Int. J. Space Struct.*, 0956059919845330, 2019.

[16] Tanaka, K., Kobayashi, S., Sato, Y., Thermomechanics of transformation pseudoelasticity and shape memory effect in alloys, *Int. J. Plast.*, vol. **2**, pp. 59–72, 1986.

[17] Wang, W., Fang, C., Liu, J., Large size superelastic SMA bars: Heat treatment strategy, mechanical property and seismic application. *Adv. Mater. Res-Switz*, vol. **25**, no. 7, 2016.

[18] Auricchio, F., Morganti, S., Reali, A., Urbano, M., Theoretical and Experimental Study of the Shape Memory Effect of Beams in Bending Conditions, *J. Mater. Eng. Perform.*, vol. **20**, no. 4, pp. 712-718, 2011. DOI:10.1007/s11665-011-9838-y

[19] Eurocode 8: Design of structures for earthquake resistance. EN1998-2. European Committee for Standardization, Bruxelles, Belgium, 2005.

[20] Cruz Sanchez, F.A., Boudaoud, H., Camargo, M., Pearce, J. M.: Plastic recycling in additive manufacturing: A systematic literature review and opportunities for the circular economy. *J Clean. Prod*, vol. **264**, 121602, 2020.